University of Sistan and Baluchestan

Challenges in Nano and Micro Scale Science and Technology

Online ISSN: 2821 - 000X

Eco-Friendly Magnetic N-doped graphene derived from orange peel for Elimination of sodium dodecyl benzenesulfonate from aqueous media

Arash Khoshnoodfar[1]✉ | Nader Bahramifar[2] | Habibollah Younesi[3]

1. Department of Environmental Engineering, Faculty of Natural Resources and Environment, University of Birjand, Birjand, University of Sistan and Baluchestan, Iran. Email: arash.khoshnoodfar69@gmail.com
2. Department of Environmental Sciences, Faculty of Natural Resources and Marine Sciences, University of Tarbiat Modares, Tehran, Iran
3. Department of Environmental Sciences, Faculty of Natural Resources and Marine Sciences, University of Tarbiat Modares, Tehran, Iran

Article Info

Article type:
Research Article

Keywords:
SDBS,
magnetic nitrogen doped graphene,
adsorption capacity,
adsorbent,
water and wastewater treatment

ABSTRACT

Surfactants such as sodium dodecylbenzene sulfonate (SDBS) are extensively used in industrial and household applications, causing serious environmental concerns due to their persistence and toxicity in aquatic systems. Conventional treatment methods are often ineffective for complete SDBS removal. To address this issue, this study introduces an eco-friendly magnetic nitrogen-doped graphene (MNG) synthesized from orange peel as an efficient and sustainable adsorbent for SDBS elimination. The aim of this research is to investigate the adsorption behavior of MNG toward SDBS in batch experiments. Various characterization techniques, including vibrating sample magnetometry (VSM), Fourier transform infrared (FTIR) spectroscopy, scanning electron microscopy (SEM), atomic force microscopy (AFM), Raman spectroscopy, elemental analysis, and Brunauer–Emmett–Teller (BET) surface area analysis, were used to confirm the successful synthesis of the nano adsorbent. The FTIR and Raman spectra verified the presence of nitrogen- and oxygen-containing functional groups and the graphitic structure of the material. SEM and AFM images revealed a wrinkled, layered morphology with a large surface area, while VSM results demonstrated strong magnetic properties enabling easy separation. The BET analysis indicated a high specific surface area suitable for efficient adsorption. Several parameters influencing adsorption performance, including adsorbent dosage, temperature, contact time, pH, and initial SDBS concentration, were systematically evaluated. The maximum adsorption capacity reached 556 mg/g at 45 °C and pH 3. The adsorption data fitted well with the Langmuir isotherm and pseudo-second-order kinetic models. Thermodynamic analysis confirmed a spontaneous and endothermic adsorption process. Moreover, SDBS could be effectively desorbed using methanol, achieving 88% desorption efficiency, and the adsorbent maintained good reusability after five cycles. This work reports, for the first time, the synthesis of magnetic N-doped graphene from orange peel, offering a promising, low-cost, and environmentally friendly material for efficient SDBS removal from contaminated water.

INTRODUCTION

Sodium dodecylbenzene sulfonate (SDBS) is an anionic surfactant widely used in detergents, textile, leather, paper, and agricultural industries due to its strong detergency, foaming, and emulsifying properties [16]. However, its extensive use and persistence in the environment have led to serious ecological problems. In municipal wastewater, SDBS concentrations typically range from 1–10 mg/L, while in industrial effluents, they may exceed 300 mg/L [15]. The discharge of SDBS into aquatic environments can cause eutrophication, foam generation, and a reduction in dissolved oxygen, posing significant risks to aquatic life and soil ecosystems [21]. Although conventional treatment methods — including physical, chemical, and biological processes, coagulation and filtration, and ion-exchange — have been widely applied to remove surfactants from

How to Cite this paper: Khoshnoodfar A. Bahramifar N. Younesi H. Eco-Friendly Magnetic N-doped graphene derived from orange peel for Elimination of sodium dodecyl benzenesulfonate from aqueous media. *Challenges in Nano and Micro Scale Science and Technology*. 2024; 12(2): 58-71. DOI: 10.22111/cnmst.2025.53384.1269

DOI: 10.22111/cnmst.2025.53384.1269

wastewater, these approaches frequently encounter fundamental limitations: low selectivity towards anionic surfactants such as Sodium Dodecylbenzene Sulfonate (SDBS), prolonged contact times, high energy or chemical input, formation of secondary waste streams, and challenging post-treatment separation operations. Recent studies have emphasized that even advanced adsorption- or membrane-based systems still struggle with cost, recovery and sustainability issues [50, 51, 52, 53]. Adsorption has emerged as a promising approach due to its simple operation, cost-effectiveness, and high efficiency in pollutant removal [42]. Numerous adsorbents such as chitosan [22], activated carbon [46], zeolites [33], and carbon nanotubes [34] have been explored for this purpose. Recently, graphene and its derivatives have attracted considerable attention owing to their large surface area, high electrical conductivity, chemical stability, and tunable surface functionalities [30]. To enhance graphene's adsorption capacity, various modification strategies have been employed, including chemical functionalization, hybridization, and heteroatom doping [37]. Among them, nitrogen doping is particularly effective, as nitrogen atoms can create chemically active sites and improve the electrical conductivity and surface reactivity of graphene [17,44, 45]. N-doped graphene (NG) has therefore shown superior adsorption properties compared to pristine graphene. However, separating NG from aqueous media after adsorption remains a significant challenge due to its fine particle size. To overcome this issue, magnetic nanoparticles (e.g., Fe_3O_4) have been integrated with NG to produce magnetic N-doped graphene (MNG), enabling facile magnetic recovery [44, 45]. Previous studies have demonstrated that the synthesis method critically influences the nanostructure, surface properties, and adsorption performance of graphene-based composites [54, 55]. Many of these methods, however, suffer from limitations such as high production costs, complex procedures, insufficient adsorption capacity, or lack of facile separation and recyclability. For example, some chemical routes produce high-quality graphene but fail to incorporate magnetic nanoparticles efficiently, while others achieve magnetization but compromise surface area and active site availability. Moreover, the use of synthetic precursors increases environmental impact and cost, limiting practical applications in wastewater treatment. To address these gaps, the present study introduces a green and cost-effective approach by using orange peel as a biomass precursor to synthesize nitrogen-doped graphene (NG), combined with in-situ incorporation of Fe_3O_4 nanoparticles to produce a magnetic nanoadsorbent (MNG). This method results in a high-surface-area, mesoporous, magnetically separable adsorbent with enhanced adsorption capacity for sodium dodecylbenzene sulfonate (SDBS). By integrating eco-friendly synthesis, structural modification via nitrogen doping, and facile magnetic recovery, this work aims to overcome the limitations of previously reported graphene-based adsorbents and provides a promising alternative for efficient removal of surfactants from contaminated water. The prepared material combines the benefits of magnetic separability, high mesoporosity, and nitrogen-doped active sites, offering an efficient, sustainable, and cost-effective adsorbent for SDBS removal. The effects of pH, adsorbent dosage, contact time, temperature, and initial SDBS concentration were systematically investigated. Furthermore, adsorption isotherms, kinetics, and thermodynamic parameters were analyzed to elucidate the adsorption mechanism. The significance of this work lies in the development of a sustainable and high-performance adsorbent synthesized via an environmentally benign process. Unlike previous studies that used non-renewable or hazardous carbon sources, this research demonstrates the first use of orange peel waste to produce magnetic N-doped graphene with enhanced adsorption capacity. The nitrogen incorporation increases surface reactivity, while Fe_3O_4 nanoparticles facilitate rapid magnetic separation and excellent reusability. Therefore, the proposed MNG effectively addresses the limitations of existing adsorbents by providing a green, low-cost, magnetically recoverable, and high-capacity solution for SDBS removal from contaminated water, contributing to sustainable wastewater treatment technologies.

Experimental

Chemicals

In this study, orange peel was selected as a suitable precursor material for the preparation of magnetic N-doped graphene (MNG) in the SDBS adsorption process. The orange peel was initially ground and then sieved through a 60 μm mesh to obtain particles of uniform size. Subsequently, the particles were thoroughly washed with distilled water to remove any impurities, and then dried in an oven at 70 °C for 48 hours until a constant weight was achieved. For the preparation and synthesis of MNG, the following chemicals were used: Sodium dodecylbenzene sulfonate ($C_{18}H_{29}SO_3Na$) was obtained from Acros in America, and Potassium hydroxide (KOH) was sourced from Scharlo in Spain. Sodium hydroxide, sulfuric acid, hydrochloric acid (37%), methanol, ethanol, sodium acetate (NaAc), ferric chloride hexahydrate ($FeCl_3.6H_2O$), ethylene glycol (EG), and urea (CH_4N_2O) were purchased from Merck in Germany. Additionally, deionized water with an electrical conductivity of 0.055 μS m^{-1} was used throughout the experiments.

N-doped graphene synthesis

To synthesize N-doped graphene, waste orange peel was used as the carbon source, and urea was used as the nitrogen source. Initially, 5 g of the carbonized sample was combined with 15 g of urea in a ratio of 3:1. The mixture was stirred on a magnetic stirrer at room temperature for 1 hour. After blending, it was dried in an oven at 110 °C for 48 hours. Next, the dried mixture was placed in a ceramic boat inside a quartz tube furnace (Nabertherm RS 80/750/11, Germany) under an argon gas flow. The temperature was raised at a rate of 5 °C per minute until it reached 700 °C, and then it was maintained at this temperature for 1 hour. Once the reaction was completed, the sample was cooled to room temperature overnight under an argon gas environment and then removed from the reactor. In the subsequent step, 5 g of the synthesized

sample was mixed with 25 g of KOH in a ratio of 1:5. The mixture was dried in an oven at 110 °C for 48 hours. The sample was then heated in a ceramic furnace under an argon gas flow with a heating rate of 10 °C per minute until it reached 900 °C. It was held at this temperature for 2 hours. Afterward, the samples were cooled under an argon gas atmosphere and removed from the reactor. The sample was further treated by stirring with 0.1 M HCl for 3 hours on a magnetic stirrer to remove the potassium hydroxide compounds. Finally, the prepared sample was filtered, washed repeatedly with deionized water until the pH reached 6-7, and dried in an oven at 110 °C for 12 hours [20].

Magnetic *N*-doped *graphene* synthesis

The preparation of Fe_3O_4-G nanoparticles was carried out using the hydrothermal method. Initially, 0.5 g of N-doped graphene (NG) powder was subjected to ultrasonication in 70 ml of ethylene glycol (C) for 3 hours. Subsequently, 0.5 g of $FeCl_3.6H_2O$ and 1 g of sodium acetate (NaAc) were added to the mixture and stirred for 30 minutes. The resulting mixture was then transferred to a Teflon-lined stainless-steel autoclave and heated at 200 °C for 10 hours. After the hydrothermal treatment, the autoclave was allowed to cool to ambient temperature. Finally, the obtained nanocomposite was thoroughly washed multiple times with distilled water and ethanol, and then vacuum-dried at -60 °C for 6 hours [1].

Characterization

Before conducting the adsorption experiments, the synthesized nanoparticles underwent several characterization techniques, including AFM (atomic force microscopy), SEM (scanning electron microscopy), BET (Brunauer-Emmett-Teller), FTIR (Fourier Transform Infrared), Raman, VSM (vibrating sample magnetometer), and elemental analysis (CHNS). The Raman spectroscopy analysis of the samples was performed using a Thermo Scientific DXR Raman Spectrometer model (USA), covering a spectral range of 200-4500 cm^{-1}. To determine the thickness of N-doped graphene sheets, AFM images were obtained using a Park Scientific CP-Research model (VEECO). Qualitative measurements to identify functional groups were conducted using a Shimadzu FT-IR 8400 spectrometer (Japan) with KBr as a background, covering a range of 4000-400 cm^{-1}. The size and morphology of the nanocomposites were observed using SEM with an LEO 1455VP microscope (Cambridge, U.K). Specific surface area and pore size distribution were calculated using BET analysis performed with a Micromeritics ASAP 2010 system (Japan). The magnetic properties of the materials at room temperature were measured using VSM from Meghnatis Daghigh Kavir Co. (Kashan, Iran). Elemental analysis of carbon, hydrogen, nitrogen, and sulfur (CHNS) was conducted to determine the weight percentages of elements. This analysis was carried out using a Thermo Finnigan Corporation Flash EA 1112 instrument for G and magnetic N-doped graphene samples.

The adsorption studies of SDBS on MNG were conducted using a batch equilibrium procedure. The experiments were carried out in 150 mL Erlenmeyer flasks, which were placed on a shaker operating at 200 rpm and maintained at a temperature of 25 °C. For each batch process, the following constant conditions were applied: a solution volume of 100 mL, SDBS concentration of 50 mg/L, adsorbent dosage of 0.1 g/L, pH value of 3, and a temperature of 45 °C. The duration of the adsorption process was 60 minutes. After the completion of the adsorption process, the magnetic nano adsorbent was separated from the solution using a magnet, and the supernatant was collected for SDBS concentration measurement. The concentration of SDBS in the solution was determined using a UV-Vis spectrophotometer (PerkinElmer Lambda 25 UV/Vis Spectrometer) at a wavelength of 223 nm. Blank samples consisting of only deionized water and prepared adsorbent were included and analyzed as a control. In the batch experiments, the effects of various parameters on SDBS removal were investigated, including adsorbent dosage, contact time, initial SDBS concentration, solution pH, and temperature. The solution pH was adjusted using HCl or NaOH. The experimental conditions were varied within the following ranges: nano adsorbent dose (0.1-0.25 g/L), temperature (15-45 °C), contact time (5-90 minutes), pH (2-10), and SDBS concentration (50-150 mg/L). To ensure accuracy, the experiments were performed with three replications, and the mean values were reported.

To assess the reusability of SDBS in batch mode, the optimal amount of MNG was added to 20 mL of methanol and ethanol as eluents. The spent nano adsorbent was then separated using a magnet, washed twice with deionized water, and dried at 70 °C for 60 minutes. Subsequently, the recycled nano adsorbent was utilized for adsorption purposes once again. The reusability of the nano adsorbent was tested under the optimized conditions. The SDBS regeneration was calculated by equation 1:

$$\text{SDBS regeneration} = \frac{\text{Amount of SDBS desorbed}}{\text{Amount of SDBS adsorbed}} \times 100 \quad (1)$$

The adsorption kinetics tests were conducted by combining 100 mL of SDBS solution with varying concentrations ranging from 50 to 150 mg/L, with a nano adsorbent dosage of 0.15 g/L. The mixture was agitated at 200 rpm and maintained at a temperature of 25 °C. The purpose of these tests was to study the adsorption kinetics and understand the mechanism of SDBS adsorption onto the MNG nano composite. To evaluate the adsorption kinetics, three models were employed: the Lagergren-first-order rate, the pseudo-second-order, and the intra-particle diffusion model (IPD). The correlation coefficient (R2), which should be close to or equal to 1, was used to assess the suitability of these models. A higher R2 value indicates a better fit of the kinetic model to the experimental data. The kinetic models provided in the following equation [1, 2]:

$$Log\ (q_e - q_t) = Log\ q_e - \frac{K_1}{2.303}\ t \quad (2)$$

$$\frac{t}{q_t} = \frac{1}{k_2 q_e^2} + \frac{t}{q_e} \quad (3)$$

where q_e and q_t (mg/g) are the amount of SDBS adsorbed at equilibrium time and amount of SDBS adsorbed at the time, respectively. k_1 (min^{-1}) and k_2 (g/mg. min) are the rate constants.

The intra-particle diffusion model (IPD), offered by Weber has been utilized for understanding to the mechanisms and rate controlling stages influencing the adsorption kinetics. The kinetic results were examined by the intra particle diffusion model to reveal the diffusion mechanism, which can be expressed as:

$$q_t = K_{id} t^{1/2} + C \quad (4)$$

where C is the intercept (mg/g) which is correlated to the boundary layer thickness and k_{id} is the slope which signifies the intra particle diffusion rate constant (mg/g $h^{1/2}$),which can be estimated from the slope of the linear plot of q_t versus $t^{1/2}$.

In order to examine the relationship between the adsorbed SDBS molecules on the nano adsorbent and the remaining concentration of SDBS in the liquid phase, the isotherm data was analyzed using the Freundlich, Langmuir, and Redlich-Peterson (R-P) models. The Langmuir isotherm model was employed to describe the equilibrium behavior between the adsorbate and adsorbent. According to this model, adsorption occurs on a homogeneous surface and is limited to a monolayer coverage without any interaction between the absorbed materials. The Langmuir model can be ascribed by equation 5 [3]:

$$q_e = \frac{q_m . b C_e}{1 + b C_e} \quad (5)$$

where C_e (mg/L) is the equilibrium concentration of SDBS solution, q_e (mg/g) is the adsorption capacity at equilibrium adsorption capacity (q_m) and b are the maximum adsorption capacity (mg/g) and the equilibrium adsorption constant (L/mg). The Freundlich model is an empirical adsorption model that offers a useful framework for understanding the relationship between the SDBS concentration on the surface of the nano adsorbent and the concentration in the aqueous phase. This isotherm model was developed to explain equilibrium adsorption in a multilayer system, assuming an exponential distribution of adsorption energies for each component. The Freundlich isotherm can be written in the linear form by equation 6 [4]:

$$q_e = K_f C_e^{1/n} \quad (6)$$

where q_e (mg/g) is the equilibrium adsorption capacity of adsorbent, C_e (mg/L) is the concentration of SDBS in liquid phase at equilibrium, K_f ((mg/g)(l/mg)$^{1/n}$) is Freundlich adsorption equilibrium constant and n is the empirical constant suggesting the intensity of adsorption which proves with the heterogeneity of adsorbent.

The Redlich-Peterson (R-P) isotherm model is commonly used to describe adsorption equilibrium across a wide concentration range. One of the advantages of this model is its versatility, as it can be applied to both homogeneous and heterogeneous systems. [5]. The Redlich–Peterson (R–P) model can be expressed by the following linear equation:

$$\ln\left(q_{RP} K_{RP} \frac{C_e}{q_e} - 1\right) = \ln K_{RP} + \beta \ln C_e \quad (7)$$

where, K_{RP} and β are the R–P constants and q_{RP} show the adsorption capacity in mg/g.

Thermodynamic investigations were carried out to assess the standard Gibbs free energy changes (ΔG0), standard enthalpy changes (ΔH0), and standard entropy changes (ΔS0) associated with the adsorption process. To determine these energy changes, adsorption experiments were conducted at different temperatures (15, 25, 35, and 45 °C). The calculations were performed using the following equation, providing insights into the thermodynamics of the adsorption process [6].

$$ln k_d = \frac{\Delta S^0}{R} - \frac{\Delta H^0}{RT} \quad (8)$$

where the k_d is equilibrium constant and its value was calculated by the ratio of q_e and C_e. ΔH^0 and ΔS^0 values were obtained from the slope and the intercept of the linear plots of ln (k_d) versus 1/T, respectively. R is the universal gas constant (8.314 J/mol.K) and T is the temperature (K). Where *K* d is the adsorption equilibrium constant and can be presented from initial and equilibrium concentration (C_o and C_e) of SDBS:

$$K_d = \frac{C_0 - C_e}{C_e} \times \frac{V}{W} \quad (9)$$

where V and W are the solution volume (mL) and the adsorbent mass (g), respectively. The ΔG^o is the change in Gibbs free energy (J/mol) and was estimated at different temperatures, which can be expressed as follows equation:

$$\Delta G^0 = \Delta H^0 - T\Delta S^0 \quad (10)$$

RESULTS AND DISCUSSION

Fourier Transform Infrared (FTIR) spectroscopy was utilized to analyze the functional groups present on the surface of the materials. The FTIR spectra of orange peel (a), G (b), MG (c), NG (d), and MNG (e) are displayed in Figure 1. Based on the figure, it can be observed that the absorption band at 3420 cm^{-1} in the FTIR spectra of orange peel and all synthesized samples corresponds to the O-H stretching vibration. Additionally, two peaks at 2858 cm^{-1} and 2925 cm^{-1} can be attributed to the symmetric and asymmetric stretching vibrations of C-H, -CH_2-NH-CH_2- or -CH_2-NH-CH_3- groups, respectively (9). The presence of peaks at 1736 cm^{-1} and 1075 cm^{-1} indicates the presence of C=O bonds from epoxy groups [43]. Furthermore, the bands located at 1248 cm^{-1} and 1384 cm^{-1} correspond to the stretching vibrations of C-N and N-CH_3, respectively, indicating an increase in nitrogen content within the graphene structure. The attachment of nitrogen atoms to the carbon lattice structure is expected to result in adsorption peaks within the range of 1200 cm^{-1} to 1600 cm^{-1} [7]. The observed peaks at 1248 cm^{-1} and 1384 cm^{-1} in the N-doped graphene spectra (curves d and e) indicate the substitution of carbon atoms with nitrogen atoms within the continuous carbon lattice. This suggests that the N-doping process in graphene sheets involves the

formation of C-N bonds. Additionally, two prominent adsorption peaks at approximately 872 cm^{-1} and 588 cm^{-1} in the N-doped graphene spectra (curves d and e) correspond to the N-H bending vibration and Fe-O stretching vibration, respectively. These findings provide confirmation of the presence of Fe3O4 magnetic nanoparticles decorating the graphene nanosheets [8, 9].

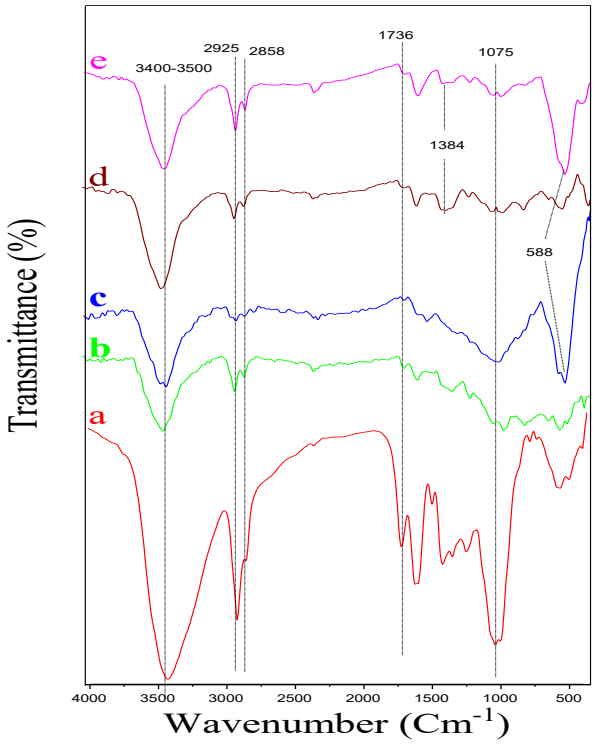

Fig. 1. FTIR spectrum of (a) orange peel, (b) G, (c) MG, (d) NG, (e) and MNG

Table 1
BET surface area (SBET), total pore volume and average pore diameters of prepared adsorbents.

Adsorbent	S_{BET} (m^2/g)	V_{total} (cm^3/g)	Micropore volume (cm^3/g)	Mesopore volume (cm^3/g)	Micropore volume (%)	D_{Ave},BJH (nm)
G	2525.1	1.4684	1.4268	0.0416	97.2	0.9
MG	1534.1	0.8014	0.7063	0.0951	88.1	0.8
GN	1640.3	0.9466	0.88	0.0666	93	0.9
MGN	1362.5	0.8081	0.72.7	0.0874	89.2	0.9

To analyze the porous structure and surface area of the synthesized adsorbents, BET analysis was conducted. The obtained results from the N2 adsorption-desorption isotherms, including the BET surface area, average pore diameters, and total pore volumes of the adsorbents (G, MG, GN, and MGN), are summarized in Table 1. The BET analysis revealed that the specific surface areas of G, MG, GN, and MGN were calculated as 2525.1, 1534.1, 1640.3, and 1362.5 m2/g, respectively. As expected, the BET surface area of the MNG adsorbent decreased due to the introduction of surface N-doping and the presence of magnetite (Fe3O4) nanoparticles within the graphene structure. According to the IUPAC adsorption-desorption isotherms, all synthesized materials exhibit a hybrid behavior combining characteristics of Type I and IV isotherms, indicating the development of mesoporosity. Raman spectroscopy, a non-destructive and powerful chemical analysis technique, provides valuable information about the number of layers, order, vibrational modes of molecules, and distinctive features of graphene-based materials. The Raman peaks associated with the synthesized materials are presented in Figure 2. It is well-established that the Raman spectra of MNG typically exhibit two prominent peaks at approximately 1561 cm^{-1} and 1339 cm^{-1}, which are assigned to the D and G peaks, respectively. The D band in the Raman spectrum is associated with the vibration of sp3 carbon atoms and indicates the presence of structural defects. On the other hand, the G band arises from the vibration of sp2 bonded carbon atoms within a graphitic domain. Additionally, the 2D band was detected at 2633 cm^{-1}, and its position is known to be sensitive to the number of graphene layers. Moreover, the layers of MNG can be determined by analyzing the intensity ratio of the 2D band to the G band, denoted as I2D/IG. Specifically, for single-layer, double-layer, triple-layer, and multi-layer (> 4) graphene, the I2D/IG intensity ratios are higher than 1.6, 0.8, 0.3, and 0.07, respectively (2,24[10, 11]. In the present investigation, the I2D/IG ratio was determined to be 0.6, indicating the presence of double or triple-layer structures in the synthesized graphene sheets. AFM imaging provides valuable information on the geometry, topology, and thickness of the prepared MNG sheets. Figure 3 shows the magnified AFM image of MNG along with a representative line scan. Height measurements indicate that the thickness of MNG nanosheets ranges from 0.8 to 1 nm, corresponding to single- to triple-layered graphene sheets. This observation confirms the high quality and few-layer structure of the synthesized MNG nanosheets. Additionally, these measurements allow estimation of the inter-lamellar distances, which are slightly larger than that of pristine graphene (~0.34 nm) due to nitrogen doping and the incorporation of Fe_3O_4 nanoparticles. The expanded interlayer spacing enhances the accessibility of SDBS molecules to internal adsorption sites, thereby improving the overall adsorption performance of the material. The magnetic properties of MG and MNG were investigated using a vibrating sample magnetometer (VSM), and the results are illustrated in Figure 4. The magnetization values of MG and MNG were determined to be 14 and 10 emu/g, respectively. The decrease in magnetization observed in the MNG sample can be attributed to the presence of nitrogen functional groups on the surface of MNG and the proportional reduction in Fe3O4 nanoparticles per unit weight. Furthermore, the magnetization curves exhibited minimal coercivity and hysteresis, indicating that both MG and MNG can be easily separated from the liquid phase after the adsorption experiment using a magnet. This confirms the strong magnetic characteristics of the prepared nanoadsorbents for the removal of SDBS. The surface morphologies of G and magnetic MNG were

examined using SEM, as depicted in Figure 5. In Figure 5a, the SEM image of the graphene nanosheets revealed thin, folded, and some crumpled structures with wrinkled edges. The SEM image of MNG (Figure 5b) exhibited the successful anchoring of Fe3O4 nanoparticles onto the surface of the graphene sheets. The average size of the Fe3O4 nanoparticles decorated on the graphene surface was estimated to be approximately 100 nm, and they displayed a uniform distribution. Furthermore, the CHNS elemental analysis of graphene and MNG is presented in Table 2. The results indicate that the carbon content in MNG slightly decreased to 86.10%, while the nitrogen content increased to 1.9% due to the presence of N-doped graphene nanosheets.

Table 2

Elemental analysis of each step of G and MNG nanosheets.

Adsorbent	Weight (%)			
	Carbon	Hydrogen	Nitrogen	Sulfur
G	95.58	0.71	0.66	0.08
MNG	86.10	0.69	1.9	0.27

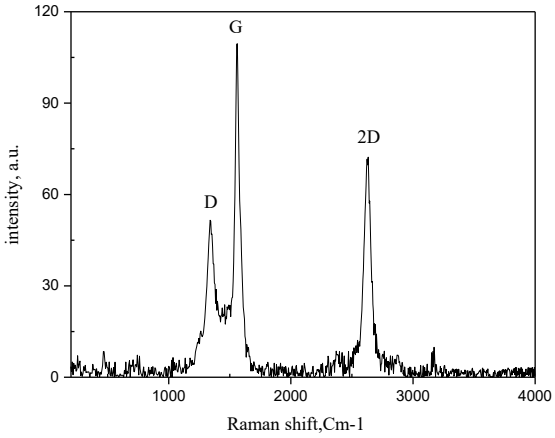

Fig. 2. Raman spectroscopy of MNG nanosheet.

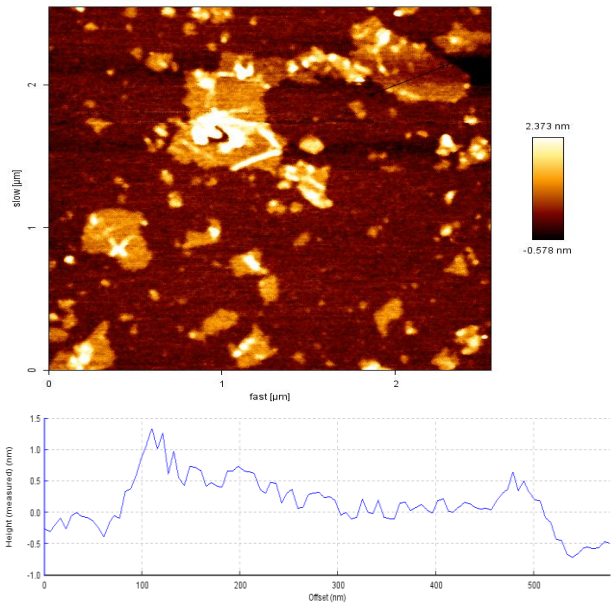

Fig. 3. AFM images of MNG nanosheet.

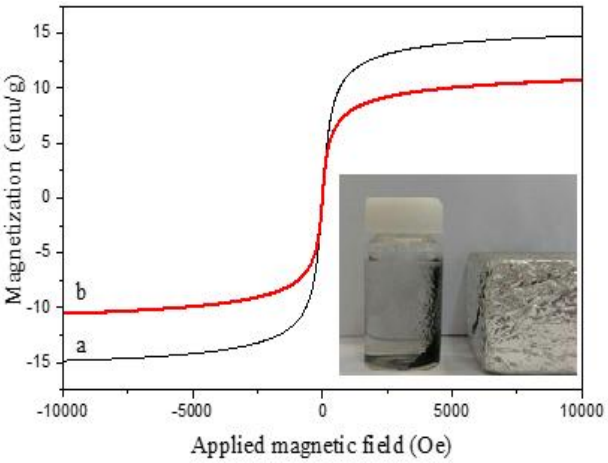

Fig. 4. VSM curves of (a) MG and (b) MNG.

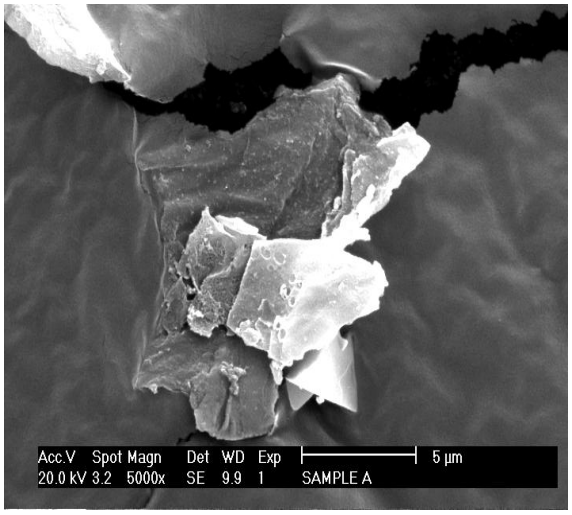

(a)

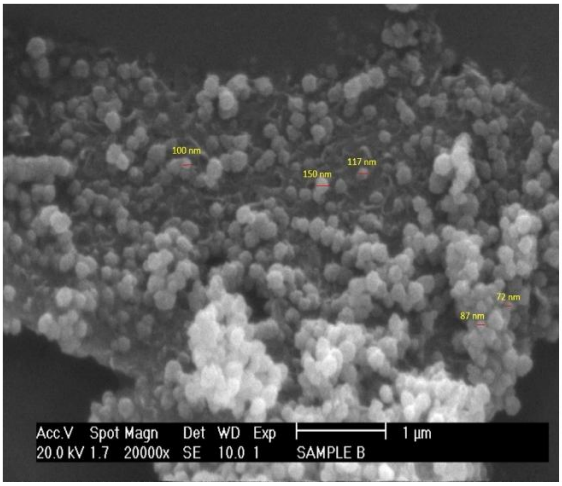

(b)

Fig. 5. SEM images of (a) G and (b) MNG.

The contact time is a crucial parameter in the adsorption process as it determines the duration required for SDBS molecules to reach equilibrium on the MNG nanocomposite. Therefore, the impact of contact time on the removal efficiency of SDBS using the synthesized nano adsorbent was investigated in the time range of 5-90 minutes, across various SDBS concentrations. The results

of the adsorption experiments are presented in Figure 6. The findings indicated that the adsorption rate of SDBS on MNG initially increased rapidly within the first 30 minutes of contact time and then approached a constant value. The equilibrium state, where 87% of SDBS was removed, was achieved at 30 minutes. Additionally, the equilibrium adsorption capacity (q_e) of MNG increased with longer contact time, reaching 217 mg/g. This increase can be attributed to the interaction between SDBS molecules and the surface functional groups of nitrogen. The rapid attainment of equilibrium can be attributed to the presence of numerous vacant sites on the surface of the nano adsorbent. However, the decrease in adsorption rate beyond 30 minutes may be associated with a low mass transfer of SDBS from the liquid phase to the surface of the MNG nanocomposite. These results align with previous studies in the literature that investigated the adsorption process of SDBS [12, 13].

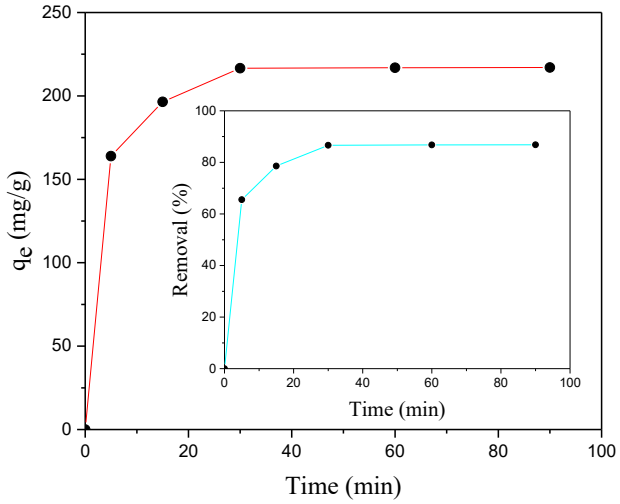

Fig. 6. Effect of contact time on SDBS adsorption onto MNG at an initial concentration of 50 mg/L and pH value of 6.5.

The pH of the solution is widely recognized as a key factor influencing the adsorption of pollutants from liquid solutions. It impacts adsorption studies by influencing the type of ions present in the solution (H^+ or OH^-) and the ionization degree of the adsorbates [15, 5]. With this in mind, the effect of different pH values (ranging from 2.0 to 10.0) on the adsorption of SDBS onto MNG nanoparticles was evaluated (Figure 9). According to Figure 7, the removal efficiency and adsorption capacity of SDBS using the synthesized nanoadsorbent increased as the pH value decreased. The highest adsorption capacity was observed at pH 2 and 3. Considering economic and environmental factors, the adsorption studies were conducted at pH 3, which was determined as the optimum pH for SDBS adsorption. Subsequent experiments were carried out at pH 3, where it was observed that the removal efficiency of SDBS reached a maximum of 94% (qe = 314 mg/g). This trend can be explained by the protonation reaction, which neutralizes negative charges and enhances the number of positive charges on the active sites of the adsorbent surface, thereby facilitating electrostatic interactions between the MNG surface and SDBS. Additionally, the presence of nitrogen groups in the structure of MNG increases the positive charges on the adsorbent surface, further improving the removal of SDBS from the aqueous solution. Conversely, at alkaline pH values, the removal rate of SDBS by MNG decreased due to stronger electrostatic repulsion. In a study by Inyinbor et al. (2016) on the removal efficiency of Rhodamine B dye using Raphiahookerie fruit epicarp as an adsorbent, higher dye removal efficiency was achieved at pH 3.0, and the adsorption capacity increased as the solution pH decreased. The removal of SDBS from the aqueous solution can be further explained by the point of zero charge (pHzpc). The pHzpc indicates the pH at which the charge on a solid surface is zero, balancing the total surface positive and negative charges on the adsorbent surface (31, 28). In this study, the pHzpc of the adsorbent was determined by introducing 10 mg of adsorbent into a 1 mM NaCl aqueous solution. Figure 8 illustrates the change in surface charges of the MNG nanoadsorbent with the pHzpc curve. The pHzpc was determined to be 7.4, indicating that the surface of the adsorbent carries a positive charge at pH values lower than 7.4 and a negative charge at pH values greater than 7.4.

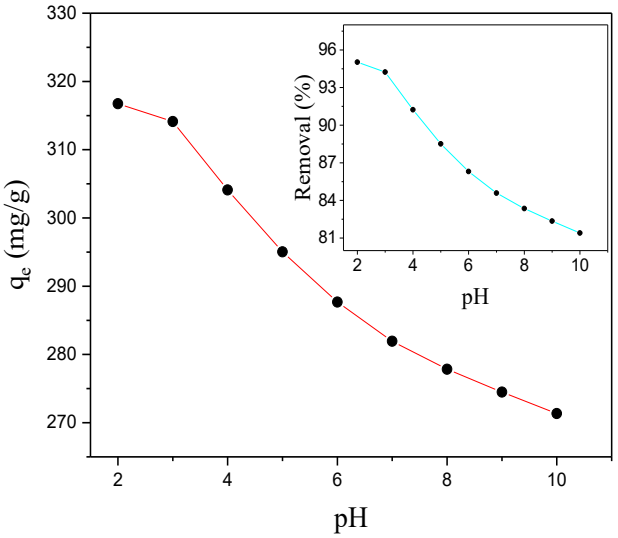

Fig. 7. Effects of solution pH on adsorption of SDBS at adsorption dosage of 15 mg, initial concentration of 50 mg/L and contact time of 30 min.

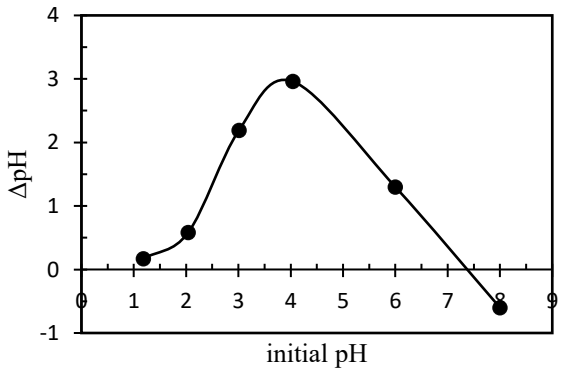

Fig. 8. pH_{pzc} of MNG.

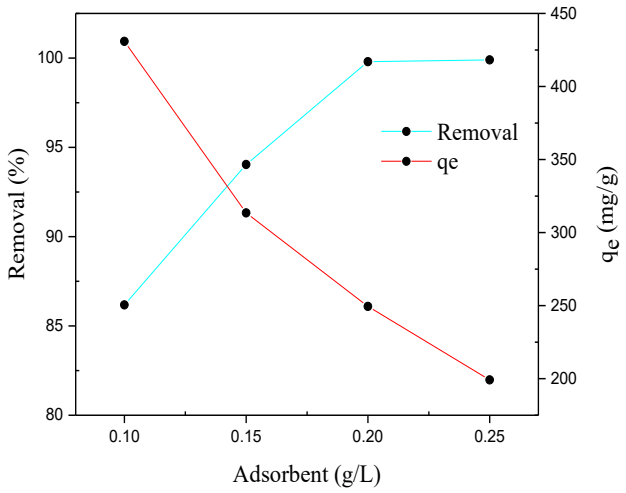

Fig. 9. Effects of different adsorbent dosages on SDBS removal by MNG at pH value of 3 and contact time of 30 min.

The impact of adsorbent dosage on the removal efficiency of SDBS using MNG was investigated, and the findings are presented in Figure 9. The results indicate that the equilibrium adsorption capacity is significantly influenced by the increase in adsorbent dosage. Under the given operating conditions, the highest removal efficiency of SDBS was achieved at an adsorbent dosage of 0.15 g/L. It was observed that as the adsorbent dosage increased from 0.1 to 0.25 g/L, the percentage of SDBS removal increased from 86% to 100%, while the equilibrium adsorption capacity (qe) decreased from 360 to 199 mg/g. This can be attributed to the greater number of available active sites on the surface of MNG at higher adsorbent dosages, resulting in more SDBS being trapped on the adsorbent surface. The results demonstrate that although the removal rate increases with an increase in adsorbent dosage, the amount of SDBS adsorbed per gram of nano adsorbent decreases. This can be explained by the insufficient saturation of available active sites for the adsorption of the pollutant. These findings are consistent with previous studies conducted by other researchers [14-16].

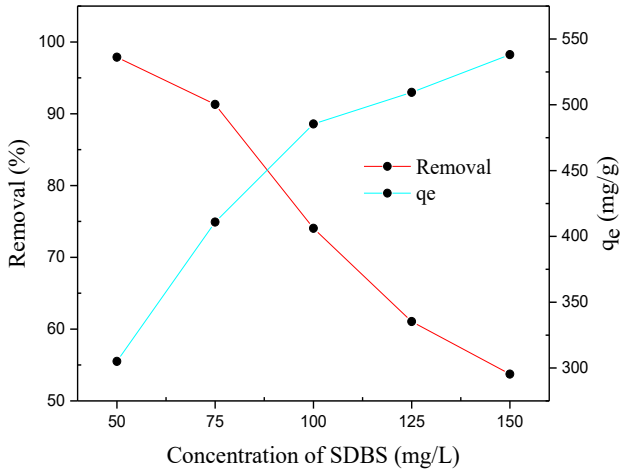

Fig. 10. Effect of initial concentration of SDBS on adsorption removal and capacity at adsorbent dosage of 15 mg, contact time of 30 min and pH value of 3.

In this section, we investigated the influence of the initial pollutant concentration on the adsorption capacity, considering the respective optimal pH. As depicted in Figure 10, increasing the concentration of SDBS from 50 to 150 mg/L resulted in a significant rise in the adsorption capacity, from 305 to 538 mg/g. This can be attributed to the increased driving force caused by the higher concentration of SDBS in the aqueous phase, leading to a greater contact between SDBS molecules and the available adsorption sites on the surface of MNG. However, it was observed that the removal percentage of SDBS by MNG decreased from 98% to 54% as the initial pollutant concentration increased. This can be explained by considering that at lower concentrations, the ratio of the initial number of molecules adsorbed to the available surface area of the nano adsorbent is substantial. In contrast, at higher concentrations, the available sites for adsorption become limited, resulting in a decrease in the removal rate of SDBS, which is dependent on the initial concentration.

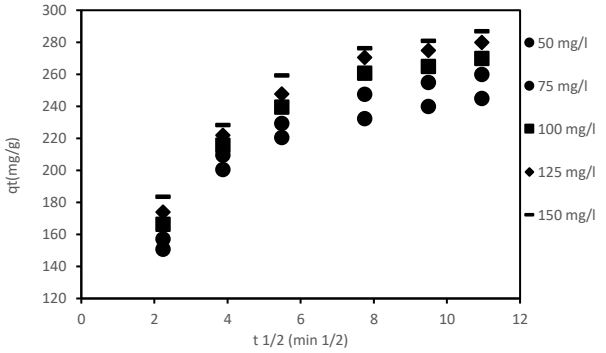

Fig.11. Kinetic models of intra particle diffusion for the adsorption of SDBS onto MNG.

To understand the mechanism of the SDBS adsorption process onto the MNG adsorbent, two linear equations, namely the pseudo-first-order and pseudo-second-order kinetic models, were employed to analyze the empirical data. The results obtained from these models are presented in Table 3. A comparison of the regression correlation coefficients ($R^2 = 0.9999$) indicated that the adsorption of SDBS molecules onto the prepared nano adsorbent followed the pseudo-second-order kinetic model more accurately than the pseudo-first-order model. It was observed that the calculated adsorption capacity (q_{e2}) from the pseudo-second-order kinetic model exhibited good agreement with the experimental values ($q_{e\ exp}$) compared to the pseudo-first-order model. This indicates that the empirical data align well with the pseudo-second-order kinetic model. The data presented in Table 3 also indicated a similar trend of decreasing pseudo-second-order constant (k_2) with increasing initial SDBS concentrations, suggesting the fast saturation of available active sites on the MNG surface by SDBS. This results in reaching equilibrium at lower initial concentrations in the adsorption system. Literature studies have also suggested that chemical adsorption processes control the reaction rate in batch systems, which involves the sharing or electron exchange between SDBS and adsorbent sites.

Consequently, covalent chemical bonds facilitate the attachment of SDBS molecules to the adsorbent surface in the solution. Similar findings were reported by Bhandari and Gogate when investigating the use of activated coconut shell as an adsorbent for SDBS removal from aqueous solutions. They observed that the adsorption of SDBS onto activated coconut shell followed the pseudo-second-order mechanism and that the adsorption process was chemisorption [3]. Robati also concluded that the pseudo-second-order model satisfactorily explained the adsorption kinetics of lead onto MWCNTs and MWCNT-COOH surfaces [25]. Additionally, based on the intraparticle diffusion diagram presented in Figure 11, the SDBS adsorption onto MNG exhibited a multilinearity, suggesting the involvement of two stages. The first stage was primarily attributed to boundary layer diffusion or macro-pore diffusion, while the second stage was related to intraparticle diffusion or micro-pore diffusion.

Table 3
Kinetic adsorption parameters obtained using pseudo-first-order and pseudo-second-order models.

			pseudo-first-order			pseudo-second-order		
Adsorbent	Conc(mg/L)	$q_{e,\,exp}$ (mg/g)	k_1 (min^{-1})	q_{e1} ($mg.g^{-1}$)	R^2	k_2 ($mg.g^{-1}.min^{-1}$)	q_{e2} ($mg.g^{-1}$)	R^2
	50	305.06	0.1131	130.62	0.7623	0.0034	312.5	0.9999
	75	410.85	0.0995	249.63	0.9031	0.0012	416.67	0.9999
	100	485.42	0.1029	310.74	0.9242	0.0009	500	1
MNG	125	509.39	0.0967	255.33	0.8205	0.0013	526.32	0.9998
	150	538.09	0.0933	254.16	0.7714	0.0012	555.56	0.9998

The adsorption isotherm models are commonly used to explain the amount of adsorbate on a surface as a function of concentration at a constant temperature. In order to understand the mechanism of SDBS adsorption onto the MNG adsorbent, three linear isotherm models, namely Langmuir, Freundlich, and Redlich-Peterson (R-P), were employed to fit the equilibrium empirical data. The fitting curves for these isotherm models are presented in Figure 12 (a, b, and c).These equilibrium isotherm models provide valuable information about the surface characteristics and adsorption capacity of the nano adsorbent. Table 4 presents the constant values and regression coefficients (R^2) obtained by fitting the empirical data to the respective isotherm models. Among the three models, the Langmuir isotherm provided the best fit for SDBS adsorption, as indicated by the high correlation coefficient value (R^2 = 0.9983). According to the literature, it can be concluded that the SDBS adsorption onto the MNG nano adsorbent occurs through monolayer coverage (uniform) and is homogeneous in nature, without any interaction between the adsorbed SDBS and the equivalent energy of all sites on the nano adsorbent surface. The Redlich-Peterson (R-P) isotherm model combines the assumptions of both the Langmuir and Freundlich models, suggesting that the adsorption mechanism is consistent with both single-layer and multi-layer adsorption. Based on the Redlich-Peterson (R-P) isotherm model, the adsorption can be classified using the Freundlich equation ($\beta > 1$) or the Langmuir equation ($\beta = 1$). In this case, the β value was estimated to be 1, indicating that the SDBS adsorption process is more in line with the Langmuir model. Consequently, the maximum adsorption capacity (q_m) for SDBS obtained from the Langmuir isotherm model was calculated to be 555.55 mg/g. Similar findings were reported by Silvio et al., who studied the adsorption of SDBS from a liquid solution using modified natural zeolite with cetyl trimethylammonium bromide (CTAB) and found that the isotherm data fit well with the Langmuir isotherm model [32]. Additionally, Vale et al. found that the adsorption of SDS and SDBS using polyvinyl chloride (PVC) had the best agreement with the Langmuir kinetic model [17].

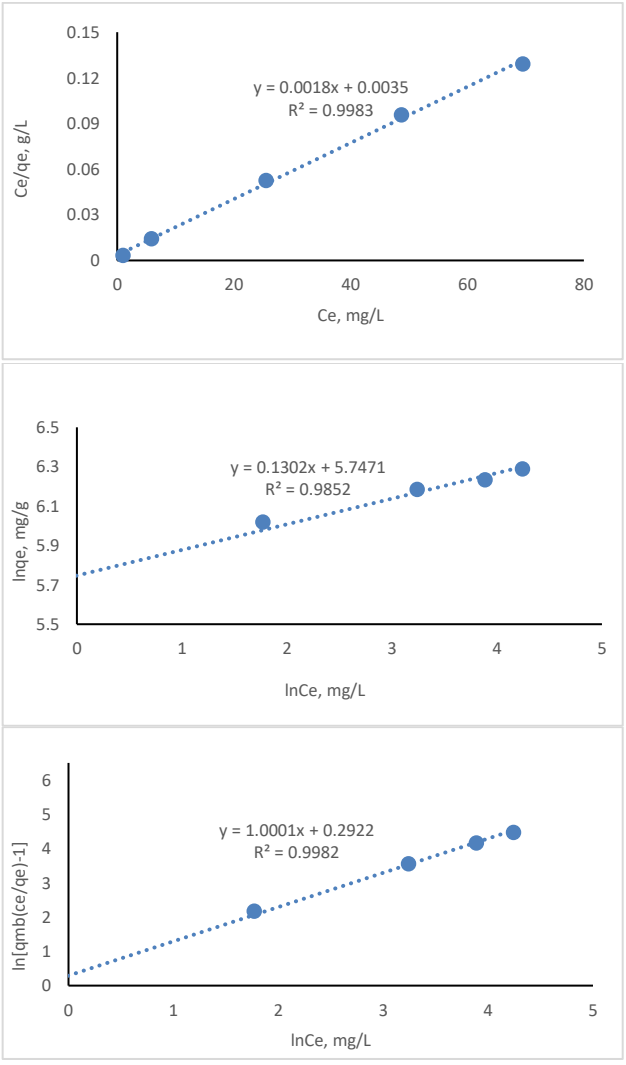

Fig. 12. The equilibrium isotherm trends for SDBS onto MNG; (a) Langmuir, (b) Freundlich, (c) Redlich-Peterson.

Table 4
Langmuir, Freundlich and Redlich–Peterson isotherm parameters for adsorption of SDBS onto MNG nanosheets.

Adsorbent	Langmuir			Freundlich			R–P			
MNG	q_m (mg/g)	b (l/g)	R^2	K_f	n	R^2	k_{RP}	a_{RP}	β	R^2
	555.55	0.0000063	0.9983	313.2808	7.68	0.9858	687	1.3394	1	0.9982

In order to understand the influence of temperature on the efficiency of SDBS removal, the thermodynamic parameters were evaluated at the studied temperatures, as presented in Table 5. The relationship between ln Kd and 1/T for the adsorption of SDBS onto MNG is shown in Figure 13. The obtained ΔH0 values, with a mean value of +59.08 J/mol, indicate that the adsorption process on the MNG nano adsorbent is endothermic, as ΔH0 is positive (ΔH0 > 0) and the Van't Hoff plot exhibits a negative slope. This finding suggests that the adsorption of SDBS onto MNG increases with rising temperature. Similar observations were reported by Zhang et al. in their studies on SDBS adsorption using modified activated carbon with ferrous sulfate [46]. The ΔH0 value was also examined to determine whether the SDBS adsorption onto the prepared nano adsorbent is physical or chemical in nature. For physical adsorption, the ΔH0 value typically falls within the range of 20-80 kJ/mol, while chemical adsorption occurs in the range of 80-400 kJ/mol [26]. Based on the estimated ΔH0 value in this study, it can be concluded that the interaction between SDBS and MNG nano adsorbent is primarily driven by physical mechanisms. Additionally, the negative value of ΔG0 (ΔG0 < 0) indicates that the adsorption of SDBS onto the magnetic nano adsorbent is spontaneous at various temperatures. In this study, the ΔG0 value ranged from -67.40 to -74.43 kJ/mol as the temperature increased from 288 to 318 K. The increasingly negative values of ΔG0 with higher temperatures suggest that the adsorption of SDBS becomes more efficient and favorable at elevated temperatures, likely due to the reduced viscosity and solubility of SDBS in the solution and the activation energy involved. Furthermore, the positive values of ΔS0 (+234.12 J/mol) can be attributed to the increased degrees of freedom of the adsorbed species in solution and the enhanced randomness at the solid-liquid interface during SDBS adsorption onto MNG. These positive ΔS0 values are also associated with structural changes in both the adsorbate and the nano adsorbent.

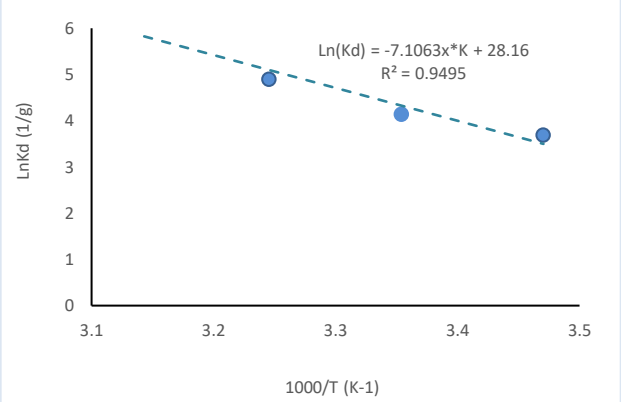

Fig. 13. The Van't Hoff equation of SDBS adsorption on MNG nanosheets.

Table 5
Thermodynamic parameters of SDBS adsorption on MNG at different temperatures

Temperature (K)	K_d (L/g)	ΔH° (J/mol)	ΔS°(J/mol)	ΔG (kJ/mol)	R^2
288	3.68	59.08	234.12	-67.40	0.9495
298	4.13			-69.74	
308	4.89			-72.09	
318	6.034			-74.43	

From a practical standpoint, the stability and regenerability of a nano adsorbent are crucial factors that contribute to reduced costs, environmental impact, and time savings. In this study, we assessed the recyclability and reusability of MNG as an adsorbent by conducting desorption experiments under batch conditions. The desorption of SDBS was carried out using 20 ml of methanol and ethanol solvents. The results showed that the desorption efficiency using methanol was 88.30%, while with ethanol it was 60.16% (Fig. 14). This indicates that SDBS can be effectively regenerated using methanol compared to ethanol. To evaluate the reusability of MNG, we performed the adsorption-desorption process for five consecutive cycles and calculated the adsorption performance for each cycle (Fig. 15). As evident from Fig. 14, the change in SDBS adsorption performance was minimal over the five cycles, with a desorption percentage of 87% after the last cycle. It is worth noting that the lower removal efficiency of MNG in subsequent adsorption-desorption cycles may be attributed to a large number of active sites on the MNG adsorbent surface remaining unoccupied by pollutants during the initial regeneration step. In subsequent steps, only a few adsorption sites are available, leading to a decrease in the efficiency of MNG. Furthermore, the magnetic properties of the MNG nano adsorbent remained intact throughout the process, allowing for easy separation and reuse of the nano adsorbent using a magnet before and after the adsorption-desorption process. Overall, our regeneration studies suggest that this nano material can be repeatedly used as an efficient adsorbent for practical applications in wastewater treatment processes.

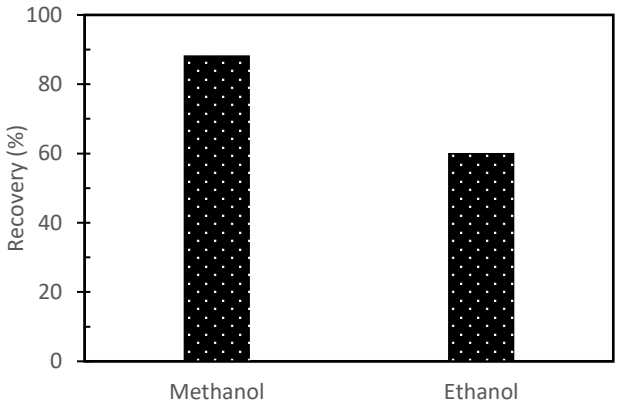

Fig. 14. Effect of solvent type on the desorption of SDBS from MNG nanosheets.

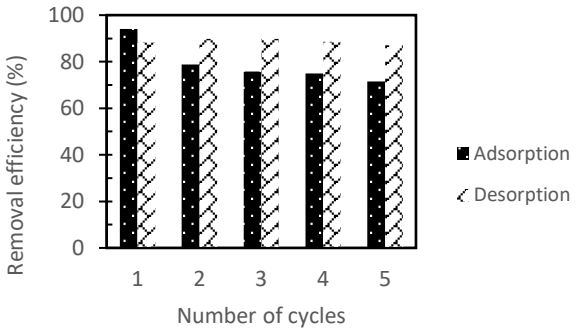

Fig. 15. The adsorption-desorption cycles of SDBS on MNG nanosheets.

The adsorption performance of SDBS onto the synthesized magnetic nitrogen-doped graphene (MNG) is strongly governed by multiple factors related to both the adsorbent properties and the solution conditions. Nitrogen doping introduces additional active sites and enhances the positive surface charge on the graphene sheets, promoting stronger electrostatic interactions with the anionic SDBS molecules. FTIR analysis confirmed the presence of C-N and N-CH_3 groups, indicating successful N incorporation, while SEM images and VSM measurements demonstrated uniform decoration of Fe_3O_4 nanoparticles with strong magnetic properties. These nanoparticles facilitate magnetic separation, enhancing recyclability, without significantly compromising adsorption sites. Elemental mapping further confirms the uniform distribution of nitrogen and iron, verifying the homogeneity and purity of the adsorbent. The adsorption process exhibits rapid initial uptake within the first 30 minutes, achieving approximately 87% removal, due to abundant vacant adsorption sites on the MNG surface. Beyond this period, the adsorption rate decreases as the active sites become partially saturated, and mass transfer limitations slow further uptake. This kinetic behavior aligns well with the pseudo-second-order model, suggesting that chemisorption mechanisms, including electron sharing between SDBS and nitrogen functional groups, play a significant role in adsorption. The pH of the solution substantially influences adsorption efficiency. Maximum removal occurs at acidic pH (2–3) due to protonation of the adsorbent surface, which increases positive surface charges and enhances electrostatic attraction with negatively charged SDBS molecules. Conversely, at alkaline pH values, electrostatic repulsion reduces adsorption efficiency. The pH point of zero charge (pHzpc = 7.4) further confirms that the MNG surface is positively charged at pH values below 7.4, facilitating SDBS uptake. To address the research gap and highlight the parameters affecting reaction yield, several factors were critically analyzed: (i) The precursor type and preparation method: Using orange peel as a renewable biomass precursor provides a highly mesoporous structure with abundant active sites, enhancing adsorption efficiency and overall yield. (ii) Reaction temperature and time: Elevated temperatures during carbonization and nitrogen doping (700–900 °C) improve the formation of high-quality graphene layers, effective nitrogen incorporation, and uniform Fe_3O_4 nanoparticle anchoring, all of which collectively increase the reaction yield. (iii) Adsorbent dosage: Higher dosages increase the total number of active sites, improving SDBS removal percentage, although adsorption capacity per gram decreases due to partial site saturation. This demonstrates the balance between total yield and per-unit efficiency. (iv) pH conditions: Acidic environments (pH 2–3) maximize protonation of nitrogen-functionalized sites, enhancing electrostatic attraction and adsorption efficiency. (v) Incorporation of Fe_3O_4 nanoparticles: These improve magnetic separability and recyclability, while slightly reducing BET surface area but compensating by increasing accessibility to active sites, ultimately enhancing effective yield. Increasing the initial SDBS concentration also increases the driving force for adsorption, resulting in higher equilibrium adsorption capacities, although the percentage removal decreases due to limited active sites relative to pollutant load. Adsorption of SDBS onto MNG is endothermic ($\Delta H > 0$), spontaneous ($\Delta G < 0$), and accompanied by increased randomness at the solid-liquid interface ($\Delta S > 0$). The positive ΔH indicates that higher temperatures facilitate SDBS uptake, likely by enhancing molecular mobility and reducing solution viscosity. The negative ΔG values suggest the feasibility of the adsorption process under the studied conditions, while positive ΔS reflects increased degrees of freedom of adsorbed molecules and structural rearrangements on the MNG surface. BET and AFM analyses reveal that MNG possesses a high surface area and mesoporous structure, which are critical for providing numerous adsorption sites. Although the introduction of N-doping and Fe_3O_4 nanoparticles slightly reduces the BET surface area, the creation of additional functional sites compensates for this loss, resulting in overall improved adsorption efficiency. Height measurements indicate that the thickness of MNG nanosheets ranges from 0.8 to 1 nm, corresponding to single- to triple-layered graphene sheets, with slightly expanded interlayer spacing due to nitrogen doping and Fe_3O_4 incorporation. This expanded spacing enhances the accessibility of SDBS molecules to internal adsorption sites. Combining the characterization results, the adsorption of SDBS on MNG can be described as a multi-stage process: (i) rapid

electrostatic attraction between SDBS molecules and positively charged nitrogen-functionalized sites, (ii) intraparticle diffusion into mesopores, and (iii) eventual equilibrium as sites become saturated. The high adsorption capacity (555–556 mg/g) observed is attributed to this synergy between structural properties, functionalization, and magnetic nanoparticle incorporation. Desorption studies demonstrate that MNG can be efficiently regenerated using methanol, with minimal loss in adsorption performance over five cycles. The magnetic properties remain intact, facilitating easy separation and reuse. Overall, the combined effects of precursor type, nitrogen doping, mesoporosity, surface functional groups, magnetic nanoparticles, pH, temperature, and adsorbent dosage dictate the adsorption performance of MNG. These parameters collectively enhance the yield and efficiency of the adsorption process, addressing the research gap, validating the importance of this study, and providing a clear rationale for the high SDBS removal observed. This comprehensive understanding also offers insights for designing future biomass-derived magnetic adsorbents with optimized performance.

CONCLUSION

In our study, we introduced a chemical method to create a highly efficient nano adsorbent derived from orange peel for the purification of SDBS from aqueous environments. The synthesized MNG was thoroughly characterized using various analyses, which confirmed the uniform decoration of iron oxide on the surface of the nitrogen-doped graphene sheet. In batch adsorption experiments, we found that the maximum SDBS removal efficiency reached 98% under the following conditions: an adsorbent dosage of 0.1 g/L, a contact time of 30 minutes, a temperature of 45°C, pH value of 3, and an initial concentration of 50 mg/L. The pH value was observed to have a significant impact on the adsorption of SDBS onto the MNG adsorbent. The experimental data further demonstrated that the adsorption kinetics followed the pseudo-second-order model, indicating favorable adsorption kinetics. The negative value of $\Delta G0$ ($\Delta G0 < 0$) and positive values of $\Delta H0$ ($\Delta H0 > 0$) confirmed the endothermic nature and spontaneous characteristics of SDBS adsorption onto the magnetic nano adsorbent. According to the Langmuir model, the maximum adsorption capacity was calculated as 556 mg/g, suggesting monolayer coverage of SDBS molecules on the surface of the nano adsorbent. Reusability studies revealed that SDBS could be efficiently and rapidly recovered from the MNG surface using a methanol solution, with a high yield of 87% after five cycles. Overall, this research offers a valuable approach for water and wastewater treatment applications due to its simplicity, reproducibility, high performance, low cost, and selectivity.

Acknowledgments

The financial support for this study was provided by Tarbiat Modares University (TMU), Iran. The authors would like to express their gratitude to the foundation of Tarbiat Modares University for their generous funding. Additionally, special thanks are extended to Mrs. Haghdoust, the Technical Assistant of the Environmental Laboratory, for her valuable assistance throughout the research process.

Competing interest

The authors declare that they have no known competing financial interests or personal relationships that could have appeared to influence the work reported in this paper.

Funding

This article was supported by the University of Tarbiat Modares (Iran) with grant code (IR-MODARES-GR-0085).

All the images in the word file of the article are of high quality, but when they are placed in the proof file, their quality decreases. Please remove the images from the word file again before printing the article.

References

[1] Ai L, Zhang C, Chen Z. Removal of methylene blue from aqueous solution by a solvothermal-synthesized graphene/magnetite composite. J Hazard Mater. 2011;192(3):1515-24.

[2] Akhavan O, Bijanzad K, Mirsepah A. Synthesis of graphene from natural and industrial carbonaceous wastes. RSC Adv. 2014;4(39):20441-8.

[3] Bhandari PS, Gogate PR. Kinetic and thermodynamic study of adsorptive removal of sodium dodecyl benzene sulfonate using adsorbent based on thermo-chemical activation of coconut shell. J Mol Liq. 2018;252:495-505.

[4] Bian Y, Bian ZY, Zhang JX, Ding AZ, Liu SL, Wang H. Effect of the oxygen-containing functional group of graphene oxide on the aqueous cadmium ions removal. Appl Surf Sci. 2015;329:269-75.

[5] Cui L, Guo X, Wei Q, Wang Y, Gao L, Yan L, et al. Removal of mercury and methylene blue from aqueous solution by xanthate functionalized magnetic graphene oxide: sorption kinetic and uptake mechanism. J Colloid Interface Sci. 2015;439:112-20.

[6] Freundlich H. Über die adsorption in lösungen. Z Phys Chem. 1907;57(1):385-470.

[7] Garcia-Delgado R, Cotoruelo L, Rodriguez J. Adsorption of anionic surfactant mixtures by polymeric resins. Sep Sci Technol. 1992;27(8-9):1065-76.

[8] Guo X, Du B, Wei Q, Yang J, Hu L, Yan L, et al. Synthesis of amino functionalized magnetic graphenes composite material and its application to remove Cr(VI), Pb(II), Hg(II), Cd(II) and Ni(II) from contaminated water. J Hazard Mater. 2014;278:211-20.

[9] Hao YM, Man C, Hu ZB. Effective removal of Cu(II) ions from aqueous solution by amino-functionalized magnetic nanoparticles. J Hazard Mater. 2010;184(1-3):392-9.

[10] Ho YS. Review of second-order models for adsorption systems. J Hazard Mater. 2006;136(3):681-9.

[11] Inyinbor A, Adekola F, Olatunji GA. Kinetics, isotherms and thermodynamic modeling of liquid phase adsorption of Rhodamine B dye onto Raphia

hookerie fruit epicarp. Water Resour Ind. 2016;15:14-27.
[12] Jiang D, Liu Q, Wang K, Qian J, Dong X, Yang Z, et al. Enhanced non-enzymatic glucose sensing based on copper nanoparticles decorated nitrogen-doped graphene. Biosens Bioelectron. 2014;54:273-8.
[13] Kahya N, Kaygusuz H, Erim FB. Aqueous removal of sodium dodecyl benzene sulfonate (SDBS) by crosslinked chitosan films. J Polym Environ. 2018;26(5):2166-72.
[14] Langmuir I. The adsorption of gases on plane surfaces of glass, mica and platinum. J Am Chem Soc. 1918;40(9):1361-403.
[15] Leyva-Ramos R, Ocampo-Pérez R, Bautista-Toledo I, Rivera-Utrilla J, Medellín-Castillo N, Aguilar-Madera C. The adsorption kinetics of sodium dodecylbenzenesulfonate on activated carbon. Chem Eng Commun. 2020;207(5):705-21.
[16] Li H, Yang Y, Gao J, Li X, Zhou Z, Wang N, et al. Degradation of sodium dodecyl benzenesulfonate by vacuum ultraviolet irradiation. J Water Process Eng. 2020;34:101172.
[17] Li SS, Lin CW, Wei KC, Huang CY, Hsu PH, Liu HL, et al. Non-invasive screening for early Alzheimer's disease diagnosis by a sensitively immunomagnetic biosensor. Sci Rep. 2016;6(1):1-11.
[18] Díaz J, Sánchez-Polo M, Rivera-Utrilla J, Bautista-Toledo M. Effectiveness of different oxidizing agents for removing sodium dodecylbenzenesulphonate in aqueous systems. Water Res. 2009;43(6):1621-9.
[19] Misra A, Tyagi PK, Rai P, Misra D. FTIR spectroscopy of multiwalled carbon nanotubes: a simple approach to study the nitrogen doping. J Nanosci Nanotechnol. 2007;7(6):1820-3.
[20] Muramatsu H, Kim YA, Yang KS, Cruz-Silva R, Toda I, Yamada T, et al. Rice husk-derived graphene with nano-sized domains and clean edges. Small. 2014;10(14):2766-70.
[21] Nazari M, Ayati B. Removing sodium dodecyl benzene sulfonate using a hybrid electrocoagulation/flotation and photocatalytic system. J Water Environ Nanotechnol. 2019;4(3):236-43.
[22] Parhizgar F, Alishahi A, Varasteh H, Rezaee H. Removing sodium dodecyl benzene sulfonate (SDBS) from aqueous solutions using chitosan. J Polym Environ. 2017;25(3):836-43.
[23] Piccin J, Dotto G, Pinto L. Adsorption isotherms and thermochemical data of FD&C Red No. 40 binding by chitosan. Braz J Chem Eng. 2011;28:295-304.
[24] Ray AK, Sahu RK, Rajinikanth V, Bapari H, Ghosh M, Paul P. Preparation and characterization of graphene and Ni-decorated graphene using flower petals as the precursor material. Carbon. 2012;50(11):4123-9.
[25] Robati D. Pseudo-second-order kinetic equations for modeling adsorption systems for removal of lead ions using multi-walled carbon nanotube. J Nanostruct Chem. 2013;3(1):55.
[26] Rodrigues LA, da Silva MLCP, Alvarez-Mendes MO, dos Reis Coutinho A, Thim GP. Phenol removal from aqueous solution by activated carbon produced from avocado kernel seeds. Chem Eng J. 2011;174(1):49-57.
[27] Saleh TA, Tuzen M, Sarı A. Polyethylenimine modified activated carbon as novel magnetic adsorbent for the removal of uranium from aqueous solution. Chem Eng Res Des. 2017;117:218-27.
[28] Sarswat A, Mohan D. Sustainable development of coconut shell activated carbon (CSAC) and magnetic coconut shell activated carbon (MCSAC) for phenol removal. RSC Adv. 2016;6(88):85390-410.
[29] Singh R, Kumar M, Khajuria H, Ladol J, Sheikh HN. Hydrothermal synthesis of magnetic Fe_3O_4–nitrogen-doped graphene hybrid composite and its application as photocatalyst in degradation of methyl orange and methylene blue dyes. Chem Pap. 2018;72(5):1181-92.
[30] Stafiej A, Pyrzynska K. Adsorption of heavy metal ions with carbon nanotubes. Sep Purif Technol. 2007;58(1):49-52.
[31] Sumalatha B, Kumar Y, Kumar K, Babu D, Narayana A, Das K, et al. Removal of indigo carmine from aqueous solution by using activated carbon. Res J Pharm Biol Chem Sci. 2014;5(2):912-22.
[32] Taffarel SR, Rubio J. Adsorption of sodium dodecyl benzene sulfonate from aqueous solution using a modified natural zeolite with CTAB. Miner Eng. 2010;23(10):771-9.
[33] Tan X, Fang M, Chen C, Yu S, Wang X. Counterion effects of nickel and sodium dodecylbenzene sulfonate adsorption to multiwalled carbon nanotubes. Carbon. 2008;46(13):1741-50.
[34] Vale HM, McKenna TF. Adsorption of sodium dodecyl sulfate and sodium dodecyl benzenesulfonate on poly(vinyl chloride) latexes. Colloids Surf A. 2005;268(1-3):68-72.
[35] Valizadeh S, Younesi H, Bahramifar N. Highly mesoporous K_2CO_3 and KOH/activated carbon for SDBS removal from water samples. Environ Nanotechnol Monit Manag. 2016;6:1-13.
[36] Wang H, Maiyalagan T, Wang X. Review on recent progress in nitrogen-doped graphene. ACS Catal. 2012;2(5):781-94.
[37] Wang S, Zhang L, Xia Z, Roy A, Chang DW, Baek JB, et al. BCN graphene as efficient metal-free electrocatalyst for the oxygen reduction reaction. Angew Chem Int Ed. 2012;51(17):4209-12.
[38] Wang Y, Shao Y, Matson DW, Li J, Lin Y. Nitrogen-doped graphene and its application in electrochemical biosensing. ACS Nano. 2010;4(4):1790-8.
[39] Wang ZL, Yan JM, Zhang YF, Ping Y, Wang HL, Jiang Q. Facile synthesis of nitrogen-doped graphene supported AuPd–CeO_2 nanocomposites. Nanoscale. 2014;6(6):3073-7.
[40] Wong S, Abd Ghafar N, Ngadi N, Razmi FA, Inuwa IM, Mat R, et al. Effective removal of anionic textile dyes using adsorbent synthesized from coffee waste. Sci Rep. 2020;10(1):1-13.

[41] Wu S, Zhang K, Wang X, Jia Y, Sun B, Luo T, et al. Enhanced adsorption of cadmium ions by 3D sulfonated reduced graphene oxide. Chem Eng J. 2015;262:1292-302.
[42] Xue B, Zhu J, Liu N, Li Y. Facile functionalization of graphene oxide with ethylenediamine. Catal Commun. 2015;64:105-9.
[43] Yang G, Li L, Rana RK, Zhu JJ. Assembled gold nanoparticles on nitrogen-doped graphene. Carbon. 2013;61:357-66.
[44] Yang HW, Lin CW, Hua MY, Liao SS, Chen YT, Chen HC, et al. Combined detection of cancer cells and a tumor biomarker. Adv Mater. 2014;26(22):3662-6.
[45] Yang X, Zhang X, Ma Y, Huang Y, Wang Y, Chen Y. Superparamagnetic graphene oxide–Fe_3O_4 nanoparticles hybrid. J Mater Chem. 2009;19(18):2710-4.
[46] Ho YS. Citation review of Lagergren kinetic rate equation on adsorption reactions. Scientometrics. 2004;59(1):171-7.
[47] Zhang L, Song X, Liu X, Yang L, Pan F, Lv J. Removal of tetracycline by multi-walled carbon nanotubes. Chem Eng J. 2011;178:26-33.
[48] Zhang Z, Deng Y, Shen M, Han W, Chen Z, Xu D, et al. Rapid degradation of sodium dodecyl benzene sulfonate under microwave irradiation. Desalination. 2009;249(3):1022-9.
[49] Mazaheri S, Monsef R, Alsultany FH, Salavati-Niasari M. Enhanced visible-light-driven photocatalytic potential of magnetic $NiMnFeO_4$/g-C_3N_4 nanocomposites. Appl Water Sci. 2025;15:130.
[50] Jafari H, Monsef R, Dawi EA, Alsultany FH, Mirzaei R, Salavati-Niasari M. Architecting diverse carbonous nanocomposites of $Sr_2V_2O_7$. Appl Water Sci. 2025;15(8):189.
[51] Khorasanizadeh MH, Monsef R, Salavati-Niasari M, Majdi HSh, Al-Azzawi WK, Hashim FS. Schiff-base ligand assisted synthesis of $DyVO_4$/AgBr nanocomposites. Arab J Chem. 2023;16:105020.
[52] Omri K, Ben Ammar L, Hamdi R, Rejaiba O, Amir Assadi A, et al. Evaluation of microstructure and mechanical properties of thermally sprayed NiCrAlY bond coats. Results Eng. 2025;26:105096.
[53] Sebaey TA, Junaedi H, Alshahrani H, Alyamani R, Akkad K. Effect of thermal aging on the crashworthiness of foam-filled CFRP composite tubes. J Mater Res Technol. 2023;23:1-12.
[54] Modigunta JKR, Park KN, Shin SC, Murali G, Udhayakumar HH, Kim J, et al. Waterborne spontaneous and robust coating of POSS nanoparticles. J Energy Storage. 2023;74:109344.